Numer. Math. Theor. Meth. Appl.
doi: 10.4208/nmtma.OA-2025-0074

Vol. **xx**, No. x, pp. 1-26
x 2026

Maximum Principle-Preserving Explicit Scheme for the Ternary Allen-Cahn Equation

Youngjin Hwang[1,2] and Junseok Kim[1,*]

[1] *Department of Mathematics, Korea University, Seoul 02841, Republic of Korea*
[2] *Department of Mathematics, Chonnam National University, Gwangju 61186, Republic of Korea*

Received 6 August 2025; Accepted (in revised version) 4 January 2026

Abstract. We investigate the stability of the ternary Allen-Cahn (tAC) equation solved by the fully explicit Euler method. The tAC equation models interface dynamics and phase separation in three-component systems, and is formulated as an L^2-gradient flow of the Ginzburg-Landau energy. We derive a sufficient condition on the time step size that satisfies the discrete maximum principle and guarantees the numerical stability of the fully explicit Euler method. Through detailed analysis, we confirm that the derived condition provides the largest possible time step size among those that preserve stability. Numerical experiments are conducted to verify the theoretical results, and the numerical solution violates the maximum principle and becomes unstable when the time step size exceeds the derived bound. Conversely, when the time step condition is satisfied, the computational solution preserves the maximum principle and maintains the energy dissipation property of the tAC equation. These results provide a rigorous theoretical foundation for determining the stability limit of the explicit Euler method applied to the tAC equation.

AMS subject classifications: 65M06, 65M12, 35K55

Key words: Stability analysis, ternary Allen-Cahn equation, maximum principle.

1. Introduction

The ternary Allen-Cahn equation plays an important role in modeling and simulating systems that consist of three distinct components [25, 44, 46]. The classical Allen-Cahn (AC) equation describes systems with two components [1], and the tAC equation extends this model to handle cases where three components coexist and influence each other. The tAC equation introduces multiple order parameters to represent different phases or components. These variables are constrained to lie within the

*Corresponding author. *Email addresses:* youngjin_hwang@korea.ac.kr (Y. Hwang), cfdkim@korea.ac.kr (J. Kim)

Gibbs simplex, which guarantees that their sum is equal to one at every point in space and time [7, 26, 36]. This mathematical structure enables the modeling of complex interfacial patterns and morphological changes arising from the interactions among three components. Many real-world phenomena in materials science [9], fluid dynamics [30, 42], crystal growth [20, 39], topology optimization [40], and biology [43] involve multi-component interactions, for which the tAC equation has been widely used. In materials science, ternary systems such as alloys with three constituents, ceramics with multiple crystalline phases, and composite materials with interpenetrating structures exhibit interfacial patterns and morphological changes involving triple junctions and curvature-driven motion [4, 27]. In biological systems, the tAC model has been used to describe cellular aggregates or tissue domains [12, 13]. In fluid dynamics, the equation has been used to model emulsions and three-phase flow systems, including droplet formation [29, 33], merging [23], and contact [21] lines among different fluid components. Various numerical studies have investigated the AC and tAC equations to develop energy-stable schemes and improve numerical accuracy. Li and Li [18] developed stabilized exponential methods for the vector-valued AC equation by applying a linear stabilization technique. The authors proved that the methods preserve the discrete maximum bound principle and dissipate the original energy, and verified their accuracy and stability through numerical simulations. Doan *et al.* [5] investigated the convergence behavior of fully discrete numerical solutions to the AC equation. They established optimal error estimates in both time and space for two first-order low regularity integrators. Li *et al.* [17] investigated the nonlocal-in-time AC equation and established its well-posedness by proving the maximal regularity for nonlocal-in-time parabolic equations with fractional power kernels. The authors also developed an energy-stable time discretization scheme and analyzed its discrete maximum principle and energy dissipation properties, which are essential in phase-field modeling. Chen *et al.* [2] developed a novel finite-difference scheme for the AC equation based on the regularized lattice Boltzmann method. In this method, the nonlinear term is treated semi-implicitly, the time derivative is discretized explicitly, and the diffusion term is approximated using second-order central differences. Under a rigorously derived time step condition, the scheme guarantees the preservation of both the discrete maximum principle and the energy dissipation law, which were verified through theoretical analysis and numerical experiments. Zhang *et al.* [45] presented third-order large time-stepping explicit schemes for the AC equation that preserve the maximum principle. The authors proposed stabilization-based Runge-Kutta-type methods, analyzed their stability and convergence theoretically, and verified temporal accuracy, energy stability, and maximum-principle preservation through numerical experiments. Du and Hou [6] developed a linear second-order finite difference method (FDM) for the generalized AC equation with nonlinear mobility and convection term. The authors proved that the stabilized Crank-Nicolson method preserves the discrete maximum bound principle under certain constraints on the time step and stabilization parameter, and verified the theoretical L^∞-error estimate through numerical experiments. Lu *et al.* [24] developed a convolution tensor decomposition-based reduced-order model for the AC equation,

combined with a stabilized semi-implicit scheme to efficiently compute high-resolution solutions while preserving the discrete energy law. This numerical method achieved significant computational speedups in two-dimensional (2D) and three-dimensional (3D) simulations of microstructure evolution. Geng *et al.* [8] proposed an end-to-end deep learning approach for solving nonlocal AC and Cahn-Hilliard (CH) equations. A neural network loss function was constructed based on the fully discrete residuals of the governing equations, and the network architecture was designed by incorporating a nonlocal kernel to address sharp interface resolution and long-range interactions. This approach achieved accurate solutions and significantly reduced computational costs in high-resolution simulations. Liu *et al.* [22] developed an efficient computational algorithm for simulating the CH equation of diblock copolymers on evolving surfaces, and they incorporated a stabilized semi-implicit method within the evolving surface finite element method to preserve mass conservation and ensure numerical stability.

In recent years, significant progress has been made in the computational modeling and simulation of multi-component systems [31], particularly in the context of phase-field models and their coupling with fluid dynamics [10]. Researchers have focused on developing efficient numerical schemes to ensure mass conservation and improve numerical stability [19, 32, 37]. Wang *et al.* [34] developed a phase-field model for triblock copolymers using the AC relaxation dynamics, in which mass conservation was achieved by introducing nonlocal Lagrange multipliers. Moreover, the authors proved the unconditional energy stability of the proposed method. Zhang and Yang [46] proposed a linear, decoupled, and non-iterative numerical scheme for a ternary Allen-Cahn-type phase-field model that conserves the volume of each phase through three nonlocal Lagrange multipliers and achieves unconditional energy stability with large time steps. The authors also verified the stability and accuracy of their method through various 2D and 3D numerical experiments. Lam and Wang [16] investigated the stability and convergence of a first-order relaxed SAV scheme for the CH equation with mass source, which may not possess a dissipative structure, and applied it to various applications such as image inpainting and tumor growth. Yang [41] developed a phase-field equation for three immiscible fluids by coupling the Navier-Stokes (NS) equations with a tAC equation using nonlocal Lagrange multipliers. The author proposed a linear, energy stable scheme based on the stabilized-IEQ and projection methods, and verified its accuracy and stability through numerical simulations. Zhang *et al.* [48] developed a phase-field-based lattice Boltzmann model for ternary fluid flows by incorporating the conservative AC equation to capture fluid interfaces and introducing a wetting boundary scheme to handle surface wettability. Wu *et al.* [35] developed the N-component conservative AC and ternary conservative Allen-Cahn-Navier-Stokes systems by introducing nonlocal Lagrange multipliers for mass conservation. The authors proposed linear, fully decoupled, and energy dissipative schemes using a modified SAV approach, and verified their accuracy and efficiency through 2D and 3D simulations. Xia *et al.* [38] proposed a conservative AC model coupled with the incompressible NS equations to study interface dynamics in multi-component immiscible fluids, including ternary systems. To suppress spurious oscillations caused by inaccurate normal vector

estimation, the authors introduced a nonlinear preprocessing step. They conducted various quantitative and qualitative computational experiments to demonstrate the accuracy and applicability of the proposed algorithm.

Although these studies have proposed various stable and efficient schemes for solving the tAC equation, the stability condition for the fully explicit Euler method has not been rigorously analyzed. In particular, while the fully explicit Euler method is simple to implement, it can become unstable when the time step is too large. Therefore, it remains an open problem to determine the largest possible time step that guarantees numerical stability and preserves physically meaningful bounds of the solution. In this study, we investigate the stability of the tAC equation solved by the fully explicit Euler method. We derive a sufficient condition on the time step size under which the computational solution satisfies the discrete maximum principle and remains stable within the physically meaningful range. Furthermore, we verify the sharpness of the derived condition and confirm its validity through numerical experiments.

The remainder of this paper is organized as follows. Section 2 introduces the mathematical formulation of the tAC equation. Section 3 presents the fully explicit Euler method and conducts the stability analysis to derive the time step constraint. Section 4 verifies the theoretical results through numerical experiments. Finally, conclusions are summarized in Section 5.

2. Governing equation

In this section, we consider a ternary phase-field model based on the Gibbs simplex method [28]. The phase variables c_1, c_2, and c_3 represent mole fractions of different components in the system, and satisfy the constraint $c_1 + c_2 + c_3 = 1$. We define the vector-valued phase-field as $\mathbf{c} = (c_1, c_2, c_3)$. The dynamics are restricted to the Gibbs simplex

$$\left\{\mathbf{c} \in \mathbb{R}^3 \mid c_1 + c_2 + c_3 = 1,\ c_p \geq 0 \ \text{ for } \ p = 1, 2, 3\right\},$$

which guarantees mass conservation and positivity of each phase-field. The Ginzburg-Landau free energy functional is given by

$$\mathcal{E}(\mathbf{c}) = \int_\Omega \sum_{p=1}^{3} \left(\frac{F(c_p(\mathbf{x}, t))}{\epsilon^2} + \frac{|\nabla c_p(\mathbf{x}, t)|^2}{2} \right) d\mathbf{x}, \tag{2.1}$$

where $F(c_p) = c_p^2(1 - c_p)^2/4$ and $\epsilon > 0$ is the interfacial coefficient. We impose the zero Neumann boundary condition

$$\nabla c_p \cdot \mathbf{n} = 0 \quad \text{on } \partial\Omega, \quad \text{for} \quad p = 1, 2, 3.$$

The time evolution of c_p for $p = 1, 2, 3$ is governed by the L^2-gradient flow of the energy functional [14]

$$\frac{\partial c_p(\mathbf{x}, t)}{\partial t} = -\frac{F'(c_p(\mathbf{x}, t))}{\epsilon^2} + \Delta c_p(\mathbf{x}, t) + \sum_{q=1}^{3} \frac{F'(c_q(\mathbf{x}, t))}{3\epsilon^2}, \quad \mathbf{x} \in \Omega, \quad t > 0, \tag{2.2}$$

where the initial condition satisfies

$$c_1(\mathbf{x},0)+c_2(\mathbf{x},0)+c_3(\mathbf{x},0)=1.$$

Moreover, the tAC equation preserves the Gibbs simplex structure over time. By differentiating the sum of the components of the tAC equation (2.2) with respect to time, we obtain

$$\begin{aligned}\frac{\partial}{\partial t}\sum_{p=1}^{3}c_p(\mathbf{x},t)&=\sum_{p=1}^{3}\frac{\partial c_p(\mathbf{x},t)}{\partial t}\\&=\sum_{p=1}^{3}\left(-\frac{F'(c_p(\mathbf{x},t))}{\epsilon^2}+\Delta c_p(\mathbf{x},t)+\sum_{q=1}^{3}\frac{F'(c_q(\mathbf{x},t))}{3\epsilon^2}\right)\\&=\sum_{p=1}^{3}\Delta c_p(\mathbf{x},t)=\Delta\left(\sum_{p=1}^{3}c_p(\mathbf{x},t)\right).\end{aligned}\tag{2.3}$$

We define the sum of the three components as $u(\mathbf{x},t)=\sum_{p=1}^{3}c_p(\mathbf{x},t)$. Then, Eq. (2.3) can be rewritten as

$$\frac{\partial u(\mathbf{x},t)}{\partial t}=\Delta u(\mathbf{x},t).\tag{2.4}$$

For the zero Neumann boundary condition, $\nabla c_p\cdot\mathbf{n}=0$ on $\partial\Omega$ for $p=1,2,3$, and thus $\nabla u\cdot\mathbf{n}=0$ on $\partial\Omega$. For the periodic boundary condition, each c_p is periodic on Ω, and therefore u is also periodic on Ω. Since the initial condition satisfies $u(\mathbf{x},0)=\sum_{p=1}^{3}c_p(\mathbf{x},0)=1$, the uniqueness of the solution to (2.4) with either homogeneous Neumann or periodic boundary conditions implies that

$$\sum_{p=1}^{3}c_p(\mathbf{x},t)=u(\mathbf{x},t)=1\quad\text{for all}\quad t>0.\tag{2.5}$$

Hence, the sum of the three components remains one for all $t>0$, and therefore the Gibbs simplex structure is preserved.

We simplify the right-hand side of the tAC equation (2.2) by computing the term $\sum_{q=1}^{3}F'(c_q(\mathbf{x},t))$

$$\begin{aligned}\sum_{q=1}^{3}F'(c_q)&=c_1(c_1-0.5)(c_1-1)+c_2(c_2-0.5)(c_2-1)+c_3(c_3-0.5)(c_3-1)\\&=c_1^3-1.5c_1^2+0.5c_1+c_2^3-1.5c_2^2+0.5c_2+c_3^3-1.5c_3^2+0.5c_3\\&=c_1^3-1.5c_1^2+c_2^3-1.5c_2^2+c_3^3-1.5c_3^2+0.5,\end{aligned}$$

and by using the constraint $c_1+c_2+c_3=1$, this expression reduces to

$$\sum_{q=1}^{3}F'(c_q)=3c_1c_2(1-c_1-c_2)=3c_1c_2c_3.\tag{2.6}$$

Therefore, the tAC equation can be rewritten in the following form for $p = 1, 2, 3$:

$$\frac{\partial c_p(\mathbf{x},t)}{\partial t} = -\frac{F'(c_p(\mathbf{x},t))}{\epsilon^2} + \Delta c_p + \frac{c_1c_2c_3}{\epsilon^2}, \quad \mathbf{x} \in \Omega, \quad t > 0. \tag{2.7}$$

We note that when $c_3 = 0$, then Eq. (2.7) reduces the classical binary AC equation [1, 15].

To verify the energy dissipation property, we differentiate the energy functional (2.1) with respect to time

$$\begin{aligned}\frac{d\mathcal{E}}{dt} &= \int_\Omega \sum_{p=1}^{3} \left(\frac{F'(c_p)}{\epsilon^2}\frac{\partial c_p}{\partial t} + \nabla c_p \cdot \nabla \left(\frac{\partial c_p}{\partial t} \right) \right) d\mathbf{x} \\ &= \int_\Omega \sum_{p=1}^{3} \left(\frac{F'(c_p)}{\epsilon^2}\frac{\partial c_p}{\partial t} - \Delta c_p \frac{\partial c_p}{\partial t} \right) d\mathbf{x},\end{aligned}$$

where integration by parts and the homogeneous Neumann boundary condition are applied to the second term. Thus, we obtain the following expression:

$$\begin{aligned}\frac{d\mathcal{E}}{dt} &= \int_\Omega \sum_{p=1}^{3} \left(\left(\frac{F'(c_p)}{\epsilon^2} - \Delta c_p \right) \frac{\partial c_p}{\partial t} \right) d\mathbf{x} \\ &= \int_\Omega \sum_{p=1}^{3} \left(\left(-\frac{\partial c_p}{\partial t} + \frac{c_1c_2c_3}{\epsilon^2} \right) \frac{\partial c_p}{\partial t} \right) d\mathbf{x} \\ &= \int_\Omega \sum_{p=1}^{3} \left(-\left(\frac{\partial c_p}{\partial t} \right)^2 + \frac{c_1c_2c_3}{\epsilon^2}\frac{\partial c_p}{\partial t} \right) d\mathbf{x} \\ &= -\int_\Omega \sum_{p=1}^{3} \left(\frac{\partial c_p}{\partial t} \right)^2 d\mathbf{x} \le 0,\end{aligned}$$

which confirms the energy dissipation property of the tAC equation.

3. Computational algorithm and stability analysis

In this section, we present the numerical method used to solve the tAC equation and perform a stability analysis of the proposed scheme. Since the numerical method can be extended to 2D and 3D spaces in a straightforward manner, we describe the one-dimensional case for ease of understanding. To discretize the tAC equation (2.2) in one-dimensional space, we discretize the finite domain $\Omega = (L_x, R_x)$ as

$$\Omega_d = \{x_i = L_x - 0.5h + ih \mid i = 1, 2, \ldots, N_x\},$$

where N_x denotes the number of grid points, and spatial step size $h = (R_x - L_x)/N_x$.

The fully explicit Euler method for the tAC equation is given by

$$\frac{c_{p,i}^{n+1}-c_{p,i}^{n}}{\Delta t}=-\frac{c_{p,i}^{n}(c_{p,i}^{n}-0.5)(c_{p,i}^{n}-1)}{\epsilon^{2}} + \frac{c_{p,i+1}^{n}+c_{p,i-1}^{n}-2c_{p,i}^{n}}{h^{2}}+\frac{c_{1,i}^{n}c_{2,i}^{n}c_{3,i}^{n}}{\epsilon^{2}}, \tag{3.1}$$

where $c_{1,i}^{0}+c_{2,i}^{0}+c_{3,i}^{0}=1$ for $i=1,\ldots,N_x$. To verify that the numerical method preserves $c_{1,i}^{n+1}+c_{2,i}^{n+1}+c_{3,i}^{n+1}=1$ for all $n\geq 0$, we first describe the boundary conditions applied to the discrete system. For the Neumann boundary condition, the discrete values satisfy $c_{p,0}^{n}=c_{p,1}^{n}$ and $c_{p,N_x+1}^{n}=c_{p,N_x}^{n}$, whereas for the periodic boundary condition, they satisfy $c_{p,0}^{n}=c_{p,N_x}^{n}$ and $c_{p,N_x+1}^{n}=c_{p,1}^{n}$. Then, based on the Gibbs simplex property of the initial conditions and the imposed Neumann or periodic boundary conditions, we obtain the following identity for all $i=1,\ldots,N_x$:

$$\sum_{p=1}^{3}\left(\frac{c_{p,i+1}^{0}+c_{p,i-1}^{0}-2c_{p,i}^{0}}{h^{2}}\right)=\frac{1}{h^{2}}\left(\sum_{p=1}^{3}c_{p,i+1}^{0}+\sum_{p=1}^{3}c_{p,i-1}^{0}-2\sum_{p=1}^{3}c_{p,i}^{0}\right)=0.$$

Therefore, by summing both sides of Eq. (3.1) over $p=1,2,3$, we obtain the following:

$$\begin{aligned}\sum_{p=1}^{3}\left(\frac{c_{p,i}^{1}-c_{p,i}^{0}}{\Delta t}\right)&=\sum_{p=1}^{3}\left(-\frac{c_{p,i}^{0}(c_{p,i}^{0}-0.5)(c_{p,i}^{0}-1)}{\epsilon^{2}}\right.\\ &\qquad\left.+\frac{c_{p,i+1}^{0}+c_{p,i-1}^{0}-2c_{p,i}^{0}}{h^{2}}+\frac{c_{1,i}^{0}c_{2,i}^{0}c_{3,i}^{0}}{\epsilon^{2}}\right)\\ &=-\sum_{p=1}^{3}\frac{c_{p,i}^{0}(c_{p,i}^{0}-0.5)(c_{p,i}^{0}-1)}{\epsilon^{2}}+\frac{3c_{1,i}^{0}c_{2,i}^{0}c_{3,i}^{0}}{\epsilon^{2}}=0,\end{aligned} \tag{3.2}$$

where the final equality follows from Eq. (2.6). Since $\Delta t>0$, Eq. (3.2) implies that

$$\sum_{p=1}^{3}c_{p,i}^{1}=\sum_{p=1}^{3}c_{p,i}^{0}=1$$

for each i. By induction on n, we conclude that

$$c_{1,i}^{n+1}+c_{2,i}^{n+1}+c_{3,i}^{n+1}=1$$

for all $n\geq 0$. To proceed with the stability analysis, we assume that the following condition holds for each $p=1,2,3$:

$$0\leq c_{p,i}^{n}\leq 1\quad\text{for}\quad i=1,2,\ldots,N_x.$$

Without loss of generality, we assume that the most restrictive time step size required to preserve the maximum principle when computing the updated solution $\mathbf{c}_{p}^{n+1}$ occurs

for $p = 1$. Rewriting the numerical scheme (3.1), we obtain

$$c_{1,i}^{n+1} = c_{1,i}^n + \Delta t \left(-\frac{c_{1,i}^n (c_{1,i}^n - 0.5)(c_{1,i}^n - 1)}{\epsilon^2} + \frac{c_{1,i+1}^n + c_{1,i-1}^n - 2c_{1,i}^n}{h^2} + \frac{c_{1,i}^n c_{2,i}^n c_{3,i}^n}{\epsilon^2} \right). \quad (3.3)$$

If the expression

$$-\frac{c_{1,i}^n (c_{1,i}^n - 0.5)(c_{1,i}^n - 1)}{\epsilon^2} + \frac{c_{1,i+1}^n + c_{1,i-1}^n - 2c_{1,i}^n}{h^2} + \frac{c_{1,i}^n c_{2,i}^n c_{3,i}^n}{\epsilon^2} = 0,$$

then the update formula reduces to $c_{1,i}^{n+1} = c_{1,i}^n$ by Eq. (3.3), and this ensures stability. To analyze the stability condition, we consider the following two cases:

$$-\frac{c_{1,i}^n (c_{1,i}^n - 0.5)(c_{1,i}^n - 1)}{\epsilon^2} + \frac{c_{1,i+1}^n + c_{1,i-1}^n - 2c_{1,i}^n}{h^2} + \frac{c_{1,i}^n c_{2,i}^n c_{3,i}^n}{\epsilon^2} > 0, \quad (3.4)$$

$$-\frac{c_{1,i}^n (c_{1,i}^n - 0.5)(c_{1,i}^n - 1)}{\epsilon^2} + \frac{c_{1,i+1}^n + c_{1,i-1}^n - 2c_{1,i}^n}{h^2} + \frac{c_{1,i}^n c_{2,i}^n c_{3,i}^n}{\epsilon^2} < 0. \quad (3.5)$$

In the first case (3.4), since $c_{1,i}^n \geq 0$, it follows that $c_{1,i}^{n+1} \geq 0$ by Eq. (3.3). Next, we consider the second case (3.5)

$$c_{1,i}^n + \Delta t \left(-\frac{c_{1,i}^n (c_{1,i}^n - 0.5)(c_{1,i}^n - 1)}{\epsilon^2} + \frac{c_{1,i+1}^n + c_{1,i-1}^n - 2c_{1,i}^n}{h^2} + \frac{c_{1,i}^n c_{2,i}^n c_{3,i}^n}{\epsilon^2} \right) \geq 0.$$

By replacing $c_{1,i+1}^n + c_{1,i-1}^n$ with its lower bound 0, we obtain

$$\Delta t \left(-\frac{c_{1,i}^n (c_{1,i}^n - 0.5)(c_{1,i}^n - 1)}{\epsilon^2} - \frac{2c_{1,i}^n}{h^2} + \frac{c_{1,i}^n c_{2,i}^n c_{3,i}^n}{\epsilon^2} \right) \geq -c_{1,i}^n. \quad (3.6)$$

When $c_{1,i}^n = 0$, the above inequality holds for any value of Δt. Therefore, we consider the case where $0 < c_{1,i}^n \leq 1$. Dividing both sides of Eq. (3.6) by $-c_{1,i}^n$ and rearranging the terms, we obtain

$$\begin{aligned} 1 &\geq \Delta t \left(\frac{(c_{1,i}^n - 0.5)(c_{1,i}^n - 1)}{\epsilon^2} + \frac{2}{h^2} - \frac{c_{2,i}^n c_{3,i}^n}{\epsilon^2} \right) \\ &= \Delta t \left(\frac{(c_{2,i}^n + c_{3,i}^n - 0.5)(c_{2,i}^n + c_{3,i}^n)}{\epsilon^2} + \frac{2}{h^2} - \frac{c_{2,i}^n c_{3,i}^n}{\epsilon^2} \right) \\ &= \Delta t \left(\frac{(c_{2,i}^n + c_{3,i}^n - 0.5)(c_{2,i}^n + c_{3,i}^n) - c_{2,i}^n c_{3,i}^n}{\epsilon^2} + \frac{2}{h^2} \right). \end{aligned}$$

To determine the maximum allowable time step size Δt, we consider the maximum value of the following expression:

$$A_i(h) = \frac{(c_{2,i}^n + c_{3,i}^n - 0.5)(c_{2,i}^n + c_{3,i}^n) - c_{2,i}^n c_{3,i}^n}{\epsilon^2} + \frac{2}{h^2}. \quad (3.7)$$

For simplicity, we define a function $g(x, y)$ by identifying $x = c_{2,i}^n$ and $y = c_{3,i}^n$ as follows:

$$g(x, y) = (x + y - 0.5)(x + y) - xy.$$

Then, the expression (3.7) can be rewritten as

$$A_i(h) = \frac{g(c_{2,i}^n, c_{3,i}^n)}{\epsilon^2} + \frac{2}{h^2}.$$

We consider the maximum value of $g(x, y)$ over the domain $0 \leq x, y < 1$ and $0 \leq x + y < 1$. To find this value, we examine the system of partial derivative equations with respect to x and y

$$\begin{cases} \dfrac{\partial g}{\partial x} = 2x + y - 0.5 = 0, \\ \dfrac{\partial g}{\partial y} = x + 2y - 0.5 = 0. \end{cases}$$

From this system, we obtain $y = -2x + 0.5$. Substituting into the second equation yields

$$x - 4x + 1 - 0.5 = -3x + 0.5 = 0,$$

which gives the solution $x = 1/6$ and $y = 1/6$. We verify whether this critical point corresponds to a local minimum or maximum. The second-order partial derivatives of $g(x, y)$ are given by

$$\frac{\partial^2 g}{\partial x^2} = 2, \quad \frac{\partial^2 g}{\partial x \partial y} = 1, \quad \frac{\partial^2 g}{\partial y^2} = 2.$$

The determinant of the Hessian matrix is

$$D = \frac{\partial^2 g}{\partial x^2}\frac{\partial^2 g}{\partial y^2} - \left(\frac{\partial^2 g}{\partial x \partial y}\right)^2 = 3 > 0 \quad \text{and} \quad \frac{\partial^2 g}{\partial x^2} = 2 > 0.$$

Therefore, the point $(x, y) = (1/6, 1/6)$ is a local minimum. Then, we consider the maximum value of $g(x, y)$ along the boundary of the domain. For $x = 0$ and $0 \leq y < 1$, we obtain $g(0, y) = (y - 0.5)y = y^2 - 0.5y$. This expression satisfies

$$\lim_{y \to 1^-} g(0, y) = \lim_{y \to 1^-} \left(y^2 - 0.5y\right) = 0.5,$$

and thus the supremum of $g(0, y)$ on the interval $[0, 1)$ is 0.5. Similarly, for $y = 0$ and $0 \leq x < 1$, we obtain

$$g(x, 0) = (x - 0.5)x = x^2 - 0.5x.$$

Thus, the supremum of $g(x, 0)$ on the interval $[0, 1)$ is 0.5. Therefore, the supremum of $g(x, y)$ over the domain $0 \leq x, y < 1$ and $0 \leq x + y < 1$ is 0.5. Substituting this into the expression for the time step condition, we obtain the following inequality for Δt:

$$1 \geq \Delta t \left(\frac{1}{2\epsilon^2} + \frac{2}{h^2}\right) = \Delta t \left(\frac{4\epsilon^2 + h^2}{2\epsilon^2 h^2}\right).$$

As a result, the maximum allowable time step size that guarantees the $c_{p,i}^{n+1} \geq 0$ is given by

$$\Delta t \leq \frac{2\epsilon^2 h^2}{h^2 + 4\epsilon^2}. \tag{3.8}$$

From Eq. (3.2), we have the identity $c_{1,i}^{n+1} + c_{2,i}^{n+1} + c_{3,i}^{n+1} = 1$. If the time step size Δt satisfies the inequality (3.8), then it follows that $0 \leq c_{1,i}^{n+1} \leq 1$. Furthermore, by using a similar approach for $p = 2, 3$, one can also conclude that $0 \leq c_{p,i}^{n+1} \leq 1$ for $p = 2, 3$. The maximum time step size is defined as

$$\Delta t_{\max} = \frac{2\epsilon^2 h^2}{h^2 + 4\epsilon^2}.$$

This value is verified to be the largest among all time step sizes that allow the computational solution to satisfy the discrete maximum principle. We assume that the inequality (3.4) holds, and then construct an example in which the computational solution fails to satisfy the maximum principle and exceeds 1. In particular, it is shown that there exists an index $i \in \{1, \ldots, N_x\}$ such that $c_{1,i}^1 > 1$ for the given initial values $c_{1,i}^0$ with $i = 1, \ldots, N_x$. First, we define a function $w(\psi_1)$ on the interval $[0.5, 1]$ as

$$w(\psi_1) = \frac{4(\psi_1 - 0.5)(2\epsilon^2 + h^2\psi_1(\psi_1 - 0.5))}{h^2 + 4\epsilon^2}, \quad \psi_1 \in [0.5, 1].$$

This function satisfies $w(0.5) = 0$ and $w(1) = 1$. The derivative of $w(\psi_1)$ is given by

$$w'(\psi_1) = \frac{8\epsilon^2 + h^2(12\psi_1^2 - 8\psi_1 + 1)}{h^2 + 4\epsilon^2}.$$

From the inequality (3.4), by taking $c_{1,i}^n = \psi_1$, $c_{2,i}^n = \psi_2$, and $c_{3,i}^n = 0$ with $\psi_1 + \psi_2 = 1$, we obtain

$$h^2\left(4(\psi_1)^2 - 2\psi_1\right) > -8\epsilon^2.$$

Thus, we obtain the following inequality on the interval $[0.5, 1]$:

$$w'(\psi_1) = \frac{8\epsilon^2 + h^2(12(\psi_1)^2 - 8\psi_1 + 1)}{h^2 + 4\epsilon^2} \geq \frac{8\epsilon^2 + h^2(4(\psi_1)^2 - 2\psi_1)}{h^2 + 4\epsilon^2} \geq 0.$$

This implies that $w'(\psi_1)$ is nonnegative and therefore $w(\psi_1)$ is monotonically increasing on the interval $[0.5, 1]$. Therefore, when the time step size Δt is greater than or equal to the maximum time step size $\Delta t_{\max}$, that is, for an exceeded time step $\Delta t \geq \Delta t_{\max}$, we can express the following relation:

$$\frac{\Delta t_{\max}}{\Delta t} = w(\psi_1), \quad \psi_1 \in [0.5, 1].$$

This implies that, for any time step size $\Delta t > \Delta t_{\max}$, there exists a value $\psi_1 \in (0.5, 1)$ such that $\Delta t = \Delta t_{\max}/w(\psi_1)$. Hence, we demonstrate that there exists an initial condition under which the numerical solution obtained from Eq. (3.3) with $\Delta t > \Delta t_{\max}$ does

not satisfy the maximum principle. We consider the initial condition on Ω_d as follows:

$$c_1(x_i,0) = \begin{cases} \psi, & \text{if} \quad i = k \quad \text{with} \quad 1 < k < N_x, \\ 1, & \text{otherwise}, \end{cases}$$
$$c_2(x_i,0) = 1 - c_1(x_i,0), \quad c_3(x_i,0) = 0,$$

where $0.5 < \psi < 1$. Then, the computational solution at time $t = \Delta t$ is computed as follows:

$$\begin{aligned} c_{1,k}^1 &= c_{1,k}^0 + \Delta t \left(- \frac{c_{1,k}^0 (c_{1,k}^0 - 0.5)(c_{1,k}^0 - 1)}{\epsilon^2} + \frac{c_{1,k+1}^0 + c_{1,k-1}^0 - 2c_{1,k}^0}{h^2} \right) \\ &= \psi + \frac{\Delta t_{\max}}{w(\psi)} \left(- \frac{\psi(\psi - 0.5)(\psi - 1)}{\epsilon^2} + \frac{2(1-\psi)}{h^2} \right) \\ &= \psi + \frac{\Delta t_{\max}}{w(\psi)\epsilon^2 h^2} \left(-h^2 \psi(\psi - 0.5)(\psi - 1) + 2\epsilon^2 (1 - \psi) \right) \\ &= \psi + \frac{(1-\psi)(h^2\psi(\psi - 0.5) + 2\epsilon^2)}{2(\psi - 0.5)\left(2\epsilon^2 + h^2\psi(\psi - 0.5)\right)} = \frac{(\psi - 1)\psi + 0.5}{\psi - 0.5} > 1, \end{aligned}$$

which implies that $c_{1,k}^{n+1} > 1$, and thus the maximum principle is not satisfied. Furthermore, since $c_{1,k}^{n+1} > 1$, it follows from Eq. (2.5) that either $c_{2,k}^{n+1}$ or $c_{3,k}^{n+1}$ becomes negative. Consequently, the maximum time step size $\Delta t_{\max}$ is the largest among all time step sizes that satisfy the maximum principle for the tAC equation solved by the fully explicit method. For a d-dimensional space, the maximum time step that preserves the stability of the explicit Euler method and satisfies the maximum principle can also be determined in the same manner, as follows:

$$\Delta t_{\max} = \frac{2\epsilon^2 h^2}{h^2 + 4d\epsilon^2}.$$

3.1. Energy stability analysis

To verify the energy stability of the numerical scheme, we define the discrete energy functionals for $\mathbf{c}_p^n = \{c_{p,1}^n, c_{p,2}^n, \ldots, c_{p,N_x}^n\}$ at time $t = n\Delta t$, for $p = 1, 2, 3$, as follows:

$$\begin{aligned} \mathcal{E}_d^{(1)}\left(\mathbf{c}_p^n\right) &= \frac{h}{4\epsilon^2} \sum_{i=1}^{N_x} \left(c_{p,i}^n\right)^2 \left(c_{p,i}^n - 1\right)^2, \\ \mathcal{E}_d^{(2)}\left(\mathbf{c}_p^n\right) &= \frac{h}{2} \sum_{i=1}^{N_x - 1} \left| \nabla_d c_{p,i+\frac{1}{2}}^n \right|^2, \\ \mathcal{E}_d\left(\mathbf{c}_p^n\right) &= \mathcal{E}_d^{(1)}\left(\mathbf{c}_p^n\right) + \mathcal{E}_d^{(2)}\left(\mathbf{c}_p^n\right). \end{aligned}$$

Thus, the discrete total energy functional corresponding to (2.1) is given by

$$\mathcal{E}_d\left(\mathbf{c}^n\right) = \sum_{p=1}^{3} \mathcal{E}_d\left(\mathbf{c}_p^n\right).$$

Then, the numerical method is expressed as follows:

$$\frac{c_{p,i}^{n+1} - c_{p,i}^n}{\Delta t} = -\frac{1}{h}\nabla \mathcal{E}_d\left(c_p^n\right)_i + \frac{c_{1,i}^n c_{2,i}^n c_{3,i}^n}{\epsilon^2} \quad \text{for} \quad p = 1, 2, 3.$$

The Hessian matrices $\mathbf{H}^{(1)}$ and $\mathbf{H}^{(2)}$, which are the second derivatives of $\mathcal{E}_d^{(1)}(\mathbf{c}_p^n)$ and $\mathcal{E}_d^{(2)}(\mathbf{c}_p^n)$, are defined by

$$\begin{aligned}
&\{\mathbf{H}^{(1)}, \mathbf{H}^{(2)}\} = \left\{\nabla^2 \mathcal{E}_d^{(1)}(\mathbf{c}_p^n), \nabla^2 \mathcal{E}_d^{(2)}(\mathbf{c}_p^n)\right\} \\
&= \left\{ \frac{h}{\epsilon^2} \begin{pmatrix} a_1^n & 0 & 0 & \dots & 0 & 0 \\ 0 & a_2^n & 0 & \dots & 0 & 0 \\ 0 & 0 & a_3^n & \dots & 0 & 0 \\ \vdots & \vdots & \vdots & \ddots & \vdots & \vdots \\ 0 & 0 & 0 & \dots & a_{N_x-1}^n & 0 \\ 0 & 0 & 0 & \dots & 0 & a_{N_x}^n, \end{pmatrix}, \; h \begin{pmatrix} 1 & -1 & 0 & \dots & 0 & 0 \\ -1 & 2 & -1 & \dots & 0 & 0 \\ 0 & -1 & 2 & \dots & 0 & 0 \\ \vdots & \vdots & \vdots & \ddots & \vdots & \vdots \\ 0 & 0 & 0 & \dots & 2 & -1 \\ 0 & 0 & 0 & \dots & -1 & 1, \end{pmatrix} \right\},
\end{aligned}$$

where $a_i^n = 3(c_{p,i}^n)^2 - 3c_{p,i}^n + 0.5$, and the homogeneous Neumann boundary condition is applied. The eigenvalues of $\mathbf{H}^{(1)}$ and $\mathbf{H}^{(2)}$ are given by

$$\lambda_i^{(1)} = \frac{h}{\epsilon^2}\left(3(c_{p,i}^n)^2 - 3(c_{p,i}^n) + 0.5\right), \quad \lambda_i^{(2)} = \frac{4}{h}\sin^2\frac{(i-1)\pi}{2N_x} \quad \text{for} \quad i = 1, \dots, N_x,$$

respectively. The eigenvectors corresponding to the eigenvalues $\lambda_i^{(2)}$ of $\mathbf{H}^{(2)}$ are given by

$$\mathbf{w}_i = \left(\cos\frac{(i-1)\pi}{2N_x}, \cos\frac{3(i-1)\pi}{2N_x}, \dots, \cos\frac{(2N_x-1)(i-1)\pi}{2N_x}\right)$$

and the normalized vectors are defined by $\mathbf{v}_i = \mathbf{w}_i/|\mathbf{w}_i|$. Thus, the difference $\mathbf{c}_p^{n+1} - \mathbf{c}_p^n$ is expressed as a linear combination of the eigenvectors

$$\mathbf{c}_p^{n+1} - \mathbf{c}_p^n = \sum_{i=1}^{N_x} s_{p,i}\mathbf{v}_i.$$

The discrete inner product $\langle \mathbf{u}, \mathbf{v}\rangle_d$ is defined as

$$\langle \mathbf{u}, \mathbf{v}\rangle_d = h\sum_{i=1}^{N_x} u_i v_i,$$

for discrete vectors $\mathbf{u} = \{u_1, u_2, \ldots, u_{N_x}\}$ and $\mathbf{v} = \{v_1, v_2, \ldots, v_{N_x}\}$. By applying the Taylor expansion of $\mathcal{E}_d$ at $\mathbf{c}_p^n$, we obtain

$$\mathcal{E}_d\left(\mathbf{c}_p^{n+1}\right) = \mathcal{E}_d\left(\mathbf{c}_p^n\right) + \left\langle \frac{\nabla \mathcal{E}_d(\mathbf{c}_p^n)}{h}, \mathbf{c}_p^{n+1} - \mathbf{c}_p^n \right\rangle_d + \left\langle \frac{\nabla^2 \mathcal{E}_d(\boldsymbol{\eta}_p)(\mathbf{c}_p^{n+1} - \mathbf{c}_p^n)}{2h}, \mathbf{c}_p^{n+1} - \mathbf{c}_p^n \right\rangle_d,$$

where $\boldsymbol{\eta}_p = \beta \mathbf{c}_p^n + (1-\beta)\mathbf{c}_p^{n+1}$ and $0 \le \beta \le 1$. We define the discrete vector $\mathbf{d}^n = \{d_1^n, d_2^n, \ldots, d_{N_x}^n\}$, where each entry is given by

$$d_i^n = c_{1,i}^n c_{2,i}^n c_{3,i}^n, \quad i = 1, 2, \ldots, N_x.$$

Then, the discrete energy difference between two time steps can be written as

$$\begin{aligned}
\mathcal{E}_d(\mathbf{c}^{n+1}) - \mathcal{E}_d(\mathbf{c}^n) &= \sum_{p=1}^{3} \left(\mathcal{E}_d(\mathbf{c}_p^{n+1}) - \mathcal{E}_d(\mathbf{c}_p^n)\right) \\
&= \sum_{p=1}^{3} \left[- \left\langle \frac{\mathbf{c}_p^{n+1} - \mathbf{c}_p^n}{\Delta t} - \frac{\mathbf{d}^n}{\epsilon^2}, \mathbf{c}_p^{n+1} - \mathbf{c}_p^n \right\rangle_d \right. \\
&\qquad \left. + \left\langle \frac{1}{2h}\left(\mathbf{H}^{(1)} + \mathbf{H}^{(2)}\right)(\mathbf{c}_p^{n+1} - \mathbf{c}_p^n), \mathbf{c}_p^{n+1} - \mathbf{c}_p^n \right\rangle_d \right] \\
&= \sum_{p=1}^{3} \left[\left\langle \left(\frac{1}{2h}\left(\mathbf{H}^{(1)} + \mathbf{H}^{(2)}\right) - \frac{1}{\Delta t} \right)(\mathbf{c}_p^{n+1} - \mathbf{c}_p^n), \mathbf{c}_p^{n+1} - \mathbf{c}_p^n \right\rangle_d \right. \\
&\qquad \left. + \left\langle \frac{\mathbf{d}^n}{\epsilon^2}, \mathbf{c}_p^{n+1} - \mathbf{c}_p^n \right\rangle_d \right]. \qquad (3.9)
\end{aligned}$$

Since the sum of concentrations satisfies $c_{1,i}^n + c_{2,i}^n + c_{3,i}^n = 1$ for all i and $n \ge 0$, it follows that

$$\sum_{p=1}^{3} \left\langle \frac{\mathbf{d}^n}{\epsilon^2}, \mathbf{c}_p^{n+1} - \mathbf{c}_p^n \right\rangle_d = \left\langle \frac{\mathbf{d}^n}{\epsilon^2}, \sum_{p=1}^{3} \left(\mathbf{c}_p^{n+1} - \mathbf{c}_p^n\right) \right\rangle_d = 0.$$

Thus, Eq. (3.9) can be rewritten as

$$\begin{aligned}
\mathcal{E}_d(\mathbf{c}^{n+1}) - \mathcal{E}_d(\mathbf{c}^n) &= \sum_{p=1}^{3} \left[\sum_{j=1}^{N_x} \sum_{i=1}^{N_x} \left\langle \left(\frac{1}{2h}\left(\lambda_i^{(1)} + \lambda_i^{(2)}\right) - \frac{1}{\Delta t} \right) s_{p,i}\mathbf{v}_i, s_{p,j}\mathbf{v}_j \right\rangle_d \right] \\
&= \sum_{p=1}^{3} \sum_{i=1}^{N_x} \left(\frac{1}{2\epsilon^2}\left(3\eta_{p,i}^2 - 3\eta_{p,i} + 0.5\right) + \frac{2}{h^2}\sin^2\frac{(i-1)\pi}{2N_x} - \frac{1}{\Delta t} \right) s_{p,i}^2.
\end{aligned}$$

If the time step size Δt satisfies $\Delta t \le 2\epsilon^2 h^2/(h^2 + 4\epsilon^2)$, then the numerical solution preserves the maximum principle, i.e., $0 \le c_{p,i}^{n+1} \le 1$ for all $i = 1, \ldots, N_x$ and $n \ge 0$.

Since each component satisfies $0 \le c_{p,i}^n, c_{p,i}^{n+1} \le 1$ and $\eta_{p,i} = \beta c_{p,i}^n + (1-\beta)c_{p,i}^{n+1}$ with $0 \le \beta \le 1$, we have $0 \le \eta_{p,i} \le 1$ for all $p = 1, 2, 3$ and $i = 1, \dots, N_x$. Therefore, the numerical method satisfies the discrete energy dissipation property as follows:

$$\mathcal{E}_d(\mathbf{c}^{n+1}) - \mathcal{E}_d(\mathbf{c}^n) \le \left(\frac{1}{4\epsilon^2} + \frac{2}{h^2} - \frac{h^2 + 4\epsilon^2}{2\epsilon^2 h^2} \right) \sum_{p=1}^{3} \sum_{i=1}^{N_x} s_{p,i}^2 = -\sum_{p=1}^{3} \sum_{i=1}^{N_x} \frac{s_{p,i}^2}{4\epsilon^2} \le 0.$$

4. Numerical tests

We perform numerical experiments to verify the presented analysis of the maximum time step for the tAC equation solved by the fully explicit Euler method. From the equilibrium profile of the AC equation, the interfacial length over which the phase-field variable varies from 0.05 to 0.95 is approximately $4\sqrt{2}\epsilon \tanh^{-1}(0.9)$. Therefore, for $m > 0$, the interfacial coefficient ϵ is chosen so that the interfacial length is approximately mh, and is given by

$$\epsilon_m = \frac{mh}{4\sqrt{2}\tanh^{-1}(0.9)}.$$

4.1. Effect of computation order on numerical stability

We take advantage of the Gibbs simplex structure, which allows us to compute only two of the three components of the tAC equation. Specifically, we compute $c_{p,ij}^n$ and $c_{q,ij}^n$ using the numerical method (3.1), and obtain the remaining component from the relation $c_{r,ij}^n = 1 - c_{p,ij}^n - c_{q,ij}^n$, where p, q, and r are distinct indices such that $1 \le p, q, r \le 3$. We perform numerical experiments to demonstrate whether the numerical solution remains unchanged under different computation orders when the proposed maximum time step size is used. In the first case, the components are denoted by $c_{p,ij}^{n+1}$ for $p = 1, 2, 3$. The numerical solutions $c_{1,ij}^{n+1}$ and $c_{2,ij}^{n+1}$ are computed using the numerical method, and the third component is then obtained by the relation $c_{3,ij}^{n+1} = 1 - c_{1,ij}^{n+1} - c_{2,ij}^{n+1}$. In the second case, the components are denoted by $\hat{c}_{p,ij}^{n+1}$ for $p = 1, 2, 3$. The numerical solutions $\hat{c}_{1,ij}^{n+1}$ and $\hat{c}_{3,ij}^{n+1}$ are first computed by the numerical method, followed by $\hat{c}_{2,ij}^{n+1} = 1 - \hat{c}_{1,ij}^{n+1} - \hat{c}_{3,ij}^{n+1}$. In the final case, the components are denoted by $\tilde{c}_{p,i}^{n+1}$ for $p = 1, 2, 3$. The numerical solutions $\tilde{c}_{2,ij}^{n+1}$ and $\tilde{c}_{3,ij}^{n+1}$ are computed by the numerical method, while $\tilde{c}_{1,ij}^{n+1} = 1 - \tilde{c}_{2,ij}^{n+1} - \tilde{c}_{3,ij}^{n+1}$ is determined from the algebraic constraint. The initial condition is imposed on the domain $\Omega = (0,1) \times (0,1)$ as follows:

$$\begin{aligned}
c_1(x, y, 0) &= \frac{1}{2} \left(\tanh \left(\frac{r_0 - \sqrt{(x-0.5)^2 + (y-0.5)^2}}{2\sqrt{2}\epsilon} \right) + 1 \right), \\
c_2(x, y, 0) &= 1 - c_1(x, y, 0) \quad \text{for} \quad y \ge 0.5, \\
c_3(x, y, 0) &= 1 - c_1(x, y, 0) \quad \text{for} \quad y < 0.5.
\end{aligned}$$

The numerical simulation is performed using the following parameters: $N_x = N_y =$

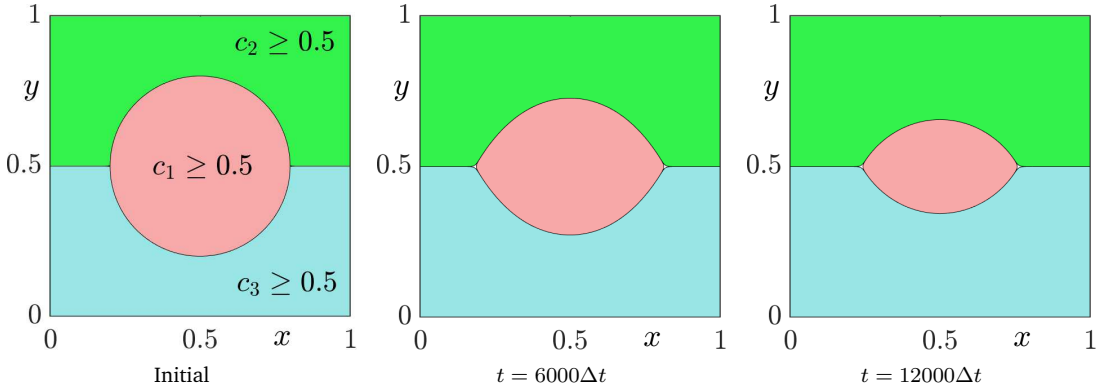

Figure 1: Temporal evolution of the numerical solution for the first case at times $t = 0$, $6000\Delta t$, and $12000\Delta t$.

256, $r_0 = 0.3$, $\epsilon = \epsilon_4$, $\Delta t = 2\epsilon^2 h^2/(h^2 + 8\epsilon^2)$, and the final time $T = 12000\Delta t$. Fig. 1 shows the temporal evolution of the numerical solution for the first case.

We define the l_2-norm of the numerical solution as follows:

$$\|c_p^n\|_2 = \left(\frac{1}{N_x N_y} \sum_{i=1}^{N_x} \sum_{j=1}^{N_y} \left(c_{p,ij}^n\right)^2 \right)^{1/2}.$$

The l_2-error between c_1^n and $\hat{c}_1^n$ is given by $\|c_1^n - \hat{c}_1^n\|_2$. The maximum l_2-error among the three numerical solutions for $p = 1, 2, 3$ is defined as

$$\mathrm{MAX}(\mathbf{e}_p^n) = \max\left(\|c_p^n - \hat{c}_p^n\|_2, \|c_p^n - \tilde{c}_p^n\|_2, \|\hat{c}_p^n - \tilde{c}_p^n\|_2\right).$$

Table 1 lists the maximum l_2-errors among the three numerical solutions for each component $p = 1, 2, 3$. Since the largest maximum l_2-error is $5.2204e$-16, it can be attributed to round-off errors in numerical computation.

Table 1: Maximum l_2-errors among the three computation orders for each component.

	$p = 1$	$p = 2$	$p = 3$
$\mathrm{MAX}(\mathbf{e}_p^n)$	$1.2899e$-16	$5.2193e$-16	$5.2204e$-16

Furthermore, to verify that the numerical solution does not exhibit any bias caused by the order of computation [11], we set the initial condition for the first case on the domain $\Omega = (0, 1) \times (0, 1)$ as follows:

$$\begin{aligned} c_1(x, y, 0) &= \frac{1}{2}\left(1 - \tanh\left(\frac{r_0 - \sqrt{(x - 0.5)^2 + (y - 0.5)^2}}{2\sqrt{2}\epsilon}\right)\right), \\ c_2(x, y, 0) &= 1 - c_1(x, y, 0) \quad \text{for} \quad y \geq 0, \\ c_3(x, y, 0) &= 1 - c_1(x, y, 0) \quad \text{for} \quad y < 0. \end{aligned} \tag{4.1}$$

The parameters used in the simulation are $N_x = N_y = 256$, $r_0 = 0.3$, $\epsilon = \epsilon_4$, $\Delta t = 2\epsilon^2 h^2/(h^2 + 8\epsilon^2)$, and the final time $T = 7000\Delta t$.

Fig. 2 shows snapshots of the numerical solution of the tAC equation with the initial condition (4.1). A magnified view near the triple junction at time $t = 7000\Delta t$, where the three components meet, is also provided. It is observed that the contact angles among the three phases converge to $120°$. This result confirms that the numerical method computes the solution without any numerical bias when the presented maximum time step size is used. Therefore, we confirm that if the time step size satisfies the discrete maximum principle, the order in which the components are computed does not affect the numerical solution. Based on this result, in the following numerical simulations, we compute $c^n_{1,ij}$ and $c^n_{2,ij}$ first, and then obtain $c^n_{3,ij} = 1 - c^n_{1,ij} - c^n_{2,ij}$ in order to preserve consistency.

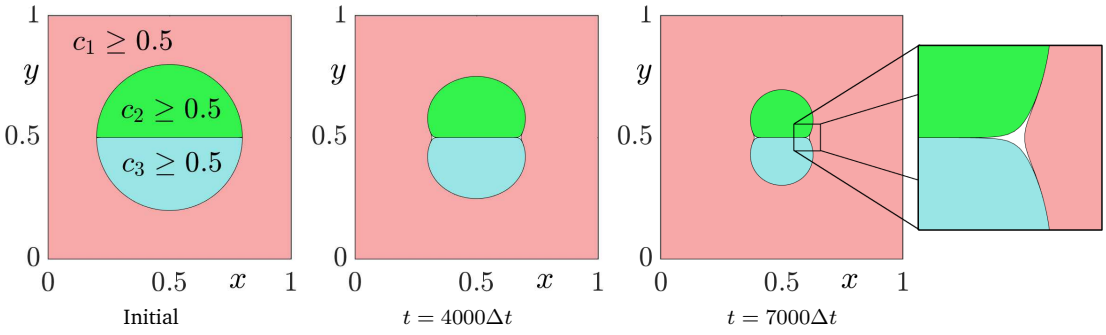

Figure 2: Snapshots of the numerical solution at times $t = 0\Delta t$, $4000\Delta t$, and $7000\Delta t$.

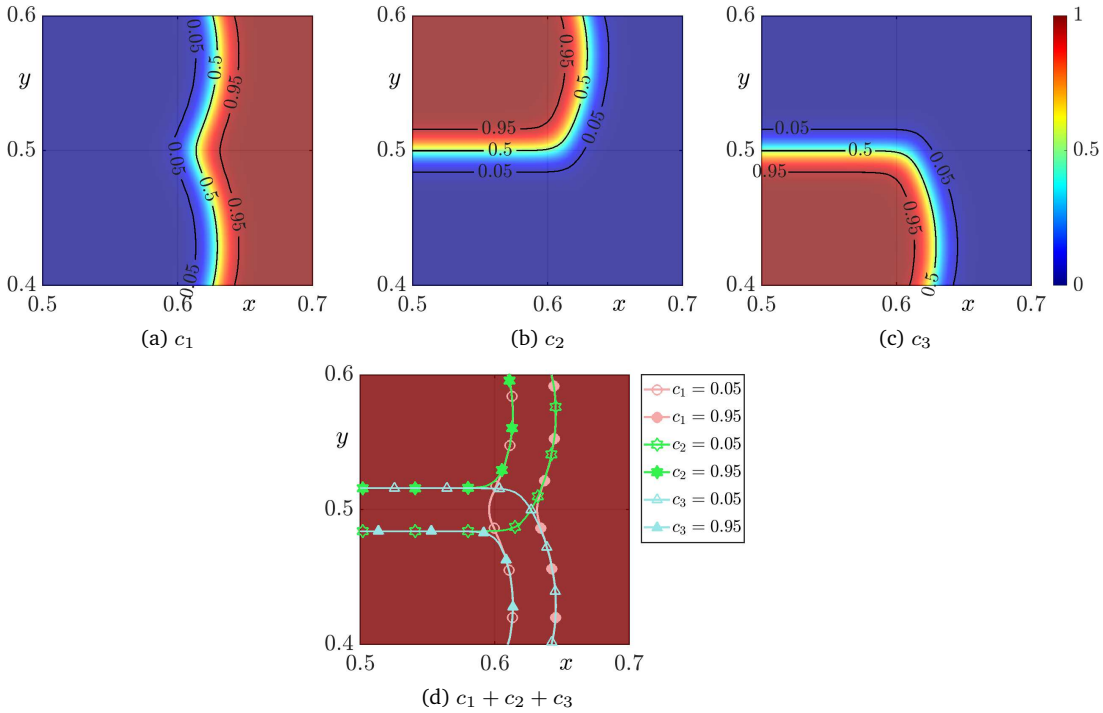

Figure 3: Numerical solutions of each component at $t = 7000\Delta t$ and their corresponding 0.05 and 0.95 level contours.

In addition, Figs. 3(a)-3(c) show the numerical solutions for the three components c_1, c_2, and c_3 at $t = 7000\Delta t$, together with their corresponding 0.05 and 0.95 level contours, respectively. Fig. 3(d) shows the sum of the computational solutions of the components, $c_1 + c_2 + c_3$, together with the 0.05 and 0.95 level contours of each component, demonstrating that the Gibbs simplex condition $c_1 + c_2 + c_3 = 1$ is numerically preserved. We observe that the small region near the triple junction in Fig. 2, which is not dominated by any of the three components, corresponds to the coexistence of all three phases with values less than 0.5 and it still satisfies the Gibbs simplex constraint.

4.2. Convergence test

The computational scheme is first-order accurate in time and second-order accurate in space. We perform convergence tests to verify these orders of accuracy. The initial condition is defined on the computational domain $\Omega = (0,1)\times(0,1)$, consisting of three independent circular interfaces, as follows:

$$
\begin{aligned}
c_1(x,y,0) = \frac{1}{3}\Bigg[1 &+ \tanh\left(\frac{r_0 - \sqrt{(x-x_1)^2+(y-y_1)^2}}{2\sqrt{2}\epsilon}\right) \\
&- \frac{1}{2}\tanh\left(\frac{r_0 - \sqrt{(x-x_2)^2+(y-y_2)^2}}{2\sqrt{2}\epsilon}\right) \\
&- \frac{1}{2}\tanh\left(\frac{r_0 - \sqrt{(x-x_3)^2+(y-y_3)^2}}{2\sqrt{2}\epsilon}\right)\Bigg], \\
c_2(x,y,0) = \frac{1}{3}\Bigg[1 &- \frac{1}{2}\tanh\left(\frac{r_0 - \sqrt{(x-x_1)^2+(y-y_1)^2}}{2\sqrt{2}\epsilon}\right) \\
&+ \tanh\left(\frac{r_0 - \sqrt{(x-x_2)^2+(y-y_2)^2}}{2\sqrt{2}\epsilon}\right) \\
&- \frac{1}{2}\tanh\left(\frac{r_0 - \sqrt{(x-x_3)^2+(y-y_3)^2}}{2\sqrt{2}\epsilon}\right)\Bigg], \\
c_3(x,y,0) &= 1 - c_1(x,y,0) - c_2(x,y,0),
\end{aligned}
$$

where $r_0 = 0.1$, and

$$
\begin{aligned}
(x_1, y_1) &= \big(0.5 - \sin(\pi/12)/4, 0.5 + \cos(\pi/12)/4\big), \\
(x_2, y_2) &= \big(0.5 + \sqrt{3}\cos(\pi/12)/8 + \sin(\pi/12)/8, 0.5 + \sqrt{3}\sin(\pi/12)/8 - \cos(\pi/12)/8\big), \\
(x_3, y_3) &= \big(0.5 - \sqrt{3}\cos(\pi/12)/8 + \sin(\pi/12)/8, 0.5 - \sqrt{3}\sin(\pi/12)/8 - \cos(\pi/12)/8\big).
\end{aligned}
$$

Since it is difficult to obtain an exact solution for the tAC equation, we generate a reference solution by using sufficiently small temporal and spatial step sizes and compare it with the numerical solution. For the spatial comparison, because the grid nodes do

Table 2: Errors and rates of the fully explicit scheme for time step size Δt.

Δt	$\Delta t_{\max}/2$		$\Delta t_{\max}/4$		$\Delta t_{\max}/8$		$\Delta t_{\max}/16$		$\Delta t_{\max}/32$
l_2-error	$3.2946e$-06		$1.6435e$-06		$8.1838e$-07		$4.0593e$-07		$1.9974e$-07
R_t		1.00		1.01		1.01		1.02	

Table 3: Errors and rates of the fully explicit scheme for grid size h.

$N_x = N_y$	32		64		128		256		512
l_2-error	$2.8113e$-03		$6.9919e$-04		$1.7276e$-04		$4.1861e$-05		$1.0355e$-05
R_s		2.01		2.02		2.05		2.02	

not coincide, linear interpolation is applied to evaluate the L_2-error at the nodal points of the numerical solution. We define the L_2-error between the numerical solution and the reference solution $\mathbf{c}^{ref} = \{c_1^{ref}, c_2^{ref}, c_3^{ref}\}$ as

$$\left\|\mathbf{e}^{N_t}_{N_x,N_y}\right\|_2 = \left(\frac{1}{3N_xN_y} \sum_{p=1}^{3} \sum_{i=1}^{N_x} \sum_{j=1}^{N_y} \left(c_p^{ref} - c_{p,ij}^{N_t} \right)^2 \right)^{1/2}.$$

Then, the convergence rates for the temporal and spatial discretizations are defined as

$$R_t = \log_2 \left(\frac{\|\mathbf{e}^{N_t}_{N_x,N_y}\|_2}{\|\mathbf{e}^{2N_t}_{N_x,N_y}\|_2} \right), \quad R_s = \log_2 \left(\frac{\|\mathbf{e}^{N_t}_{N_x,N_y}\|_2}{\|\mathbf{e}^{N_t}_{2N_x,2N_y}\|_2} \right).$$

The reference solution for the temporal convergence test is generated using $\Delta t = \Delta t_{\max}/1024$, $N_x = N_y = 1024$, $T = 2^{16}\Delta t$, and $\epsilon = 0.004$. For the temporal convergence test, we use the parameters $N_x = 1024$, $\epsilon = 0.004$, different time step sizes $\Delta t = \Delta t_{\max}/2$, $\Delta t_{\max}/4$, $\Delta t_{\max}/8$, $\Delta t_{\max}/16$, and $\Delta t_{\max}/32$, and the final time $T = 64\Delta t_{\max}$. Table 2 lists the L_2-errors and the corresponding convergence rates of the fully explicit scheme for different time step sizes. The reference solution for the spatial convergence test is generated using $\Delta t = \Delta t_{\max}/4$, $N_x = N_y = 1024$, $T = 2^{14}\Delta t$, and $\epsilon = 0.01$. For the spatial convergence test, we use the parameters $\Delta t = \Delta t_{\max}/4$, $\epsilon = 0.01$, different spatial step sizes $N_x = 32, 64, 128, 256$, and 512, and the final time $T = 2^{14}\Delta t$. Table 3 lists the L_2-errors and the corresponding convergence rates of the fully explicit scheme for different grid sizes.

4.3. Stability test

We demonstrate through numerical simulations that when the time step size exceeds the maximum allowable value, the numerical solution fails to satisfy the maximum principle and becomes unstable. To quantify this behavior, we define the maximum and minimum values of the numerical solution at time $t = n\Delta t$ as follows:

$$\mathrm{Max}(\mathbf{c}^n) = \max_{1\le p\le 3} \big(\max_{(x_i,y_j)\in\Omega_d} c^n_{p,ij} \big), \quad \mathrm{Min}(\mathbf{c}^n) = \min_{1\le p\le 3} \big(\min_{(x_i,y_j)\in\Omega_d} c^n_{p,ij} \big).$$

The initial condition on the domain $\Omega = (0,1) \times (0,1)$ is defined by uniformly distributing each component around $1/3$ with a small random perturbation

$$\begin{aligned} c_1(x,y,0) &= \frac{1}{3} + 0.01\text{rand}(x,y), \\ c_2(x,y,0) &= \frac{1}{3} + 0.01\text{rand}(x,y), \\ c_3(x,y,0) &= 1 - c_1(x,y,0) - c_2(x,y,0), \end{aligned}$$

where $\text{rand}(x,y)$ denotes a uniformly distributed random value in $(-1,1)$ at each spatial point (x,y). The simulation is conducted with $N_x = N_y = 256$, $\epsilon = \epsilon_4$, and the final time $T = 5.0448e\text{-}3$. We use two time step sizes, $\Delta t = \Delta t_{\max}$ and $\Delta t = 1.1\Delta t_{\max}$, to examine the effect of violating the stability condition.

Figs. 4(a) and 4(b) show snapshots of the numerical solutions at times $t = 5.9192e\text{-}4$, $1.8497e\text{-}3$, and $4.8093e\text{-}3$, respectively. Fig. 4(c) shows the numerical solutions $c^n_{1,ij}$ and $c^n_{2,ij}$ at $t = 4.8093e\text{-}3$ along the fixed line $j = N_y/2$ for both $\Delta t = \Delta t_{\max}$ and $\Delta t = 1.1\Delta t_{\max}$. Since $c^n_{3,ij} = 1 - c^n_{1,ij} - c^n_{2,ij}$, it is omitted for visualization. We observed that the numerical solution satisfies the maximum principle and remains stable when the time step size Δt is set to the presented maximum time step size $\Delta t_{\max}$. In contrast, if the time step size Δt exceeds this threshold, the solution fails to satisfy the maximum principle, exhibits oscillatory behavior, and becomes unstable. Fig. 4(d) shows the temporal evolution of the maximum and minimum values of the numerical solution, which clearly illustrates this behavior.

4.4. Energy dissipation law

We perform numerical simulations to demonstrate whether the numerical solution of the tAC equation satisfies the energy dissipation law when the time step size Δt is set to the presented maximum time step size $\Delta t_{\max}$. The discrete total energy of the numerical solution $\mathbf{c}^n$ at time $t = n\Delta t$ is defined as follows:

$$\mathcal{E}_d(\mathbf{c}^n) = \sum_{i=1}^{N_x} \sum_{j=1}^{N_y} \sum_{p=1}^{3} \left(\frac{F(c^n_{p,ij})}{\epsilon^2} + \frac{(c^n_{p,i+1,j} - c^n_{p,ij})^2 + (c^n_{p,i,j+1} - c^n_{p,ij})^2}{2h^2} \right) h^2.$$

We consider the following initial condition on the domain $\Omega = (0,1) \times (0,1)$:

$$\begin{aligned} c^n_{1,ij} &= 0.5\big(1 + \text{rand}_1(x_i, y_j)\big), \\ c^n_{2,ij} &= 0.5\big(\text{rand}_2(x_i, y_j) - \text{rand}_1(x_i, y_j)\big), \\ c^n_{3,ij} &= 1 - 0.5\big(1 + \text{rand}_2(x_i, y_j)\big), \end{aligned}$$

where the uniformly distributed random values satisfy $\text{rand}_1(x_i, y_j) \le \text{rand}_2(x_i, y_j)$ at each point (x_i, y_j) to preserve consistency. We use the parameters $N_x = N_y = 256$, $\epsilon = \epsilon_4$, $\Delta t = 2\epsilon^2 h^2/(h^2 + 8\epsilon^2)$, and the final time $T = 2000\Delta t$.

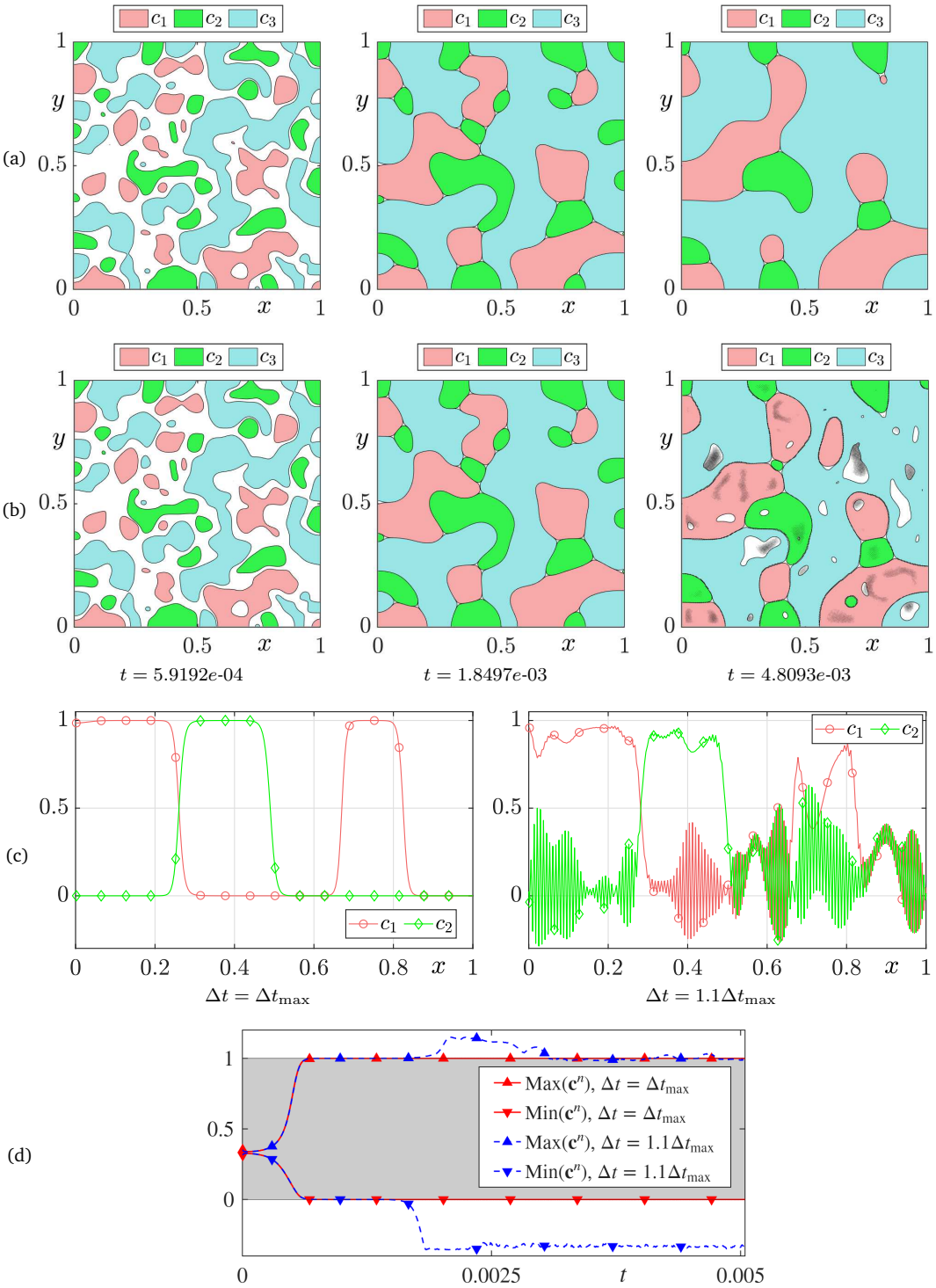

Figure 4: Snapshots and temporal evolution of the maximum and minimum values of the numerical solution for different time step sizes $\Delta t = \Delta t_{\max}$ and $\Delta t = 1.1\Delta t_{\max}$.

Fig. 5 shows snapshots of the computational solution at times $t = 80\Delta t$, $400\Delta t$, and $2000\Delta t$, along with the temporal evolution of the normalized discrete total energy $\mathcal{E}_d(\mathbf{c}^n)/\mathcal{E}_d(\mathbf{c}^1)$. We observed that the normalized discrete energy decreases over time, which demonstrates that the computational solution satisfies the energy dissipation law of the tAC equation.

Next, we conduct computational simulations in 3D space to verify whether the numerical solutions of the tAC equation satisfy the maximum principle and the energy dissipation law based on the presented analysis. The initial conditions are given as follows:

$$
\begin{aligned}
c^n_{1,ijk} &= 0.5\big(1 + \text{rand}_1(x_i, y_j, z_k)\big),\\
c^n_{2,ijk} &= 0.5\big(\text{rand}_2(x_i, y_j, z_k) - \text{rand}_1(x_i, y_j, z_k)\big),\\
c^n_{3,ijk} &= 1 - 0.5\big(1 + \text{rand}_2(x_i, y_j, z_k)\big).
\end{aligned}
$$

The parameters used in the simulations are $N_x = N_y = N_z = 128$, $\epsilon = \epsilon_4$, $\Delta t = 2\epsilon^2 h^2/(h^2 + 12\epsilon^2)$, and the final time $T = 3000\Delta t$. Figs. 6(a)-6(c) present snapshots of the numerical solutions at $t = 300\Delta t$, $1000\Delta t$, and $3000\Delta t$. The numerical solutions are stable without oscillations, and each component follows the motion by mean curvature flow, which is a property of the AC equation. In addition, Fig. 6(d) presents the maximum and minimum values of the computational solutions. We observe that the

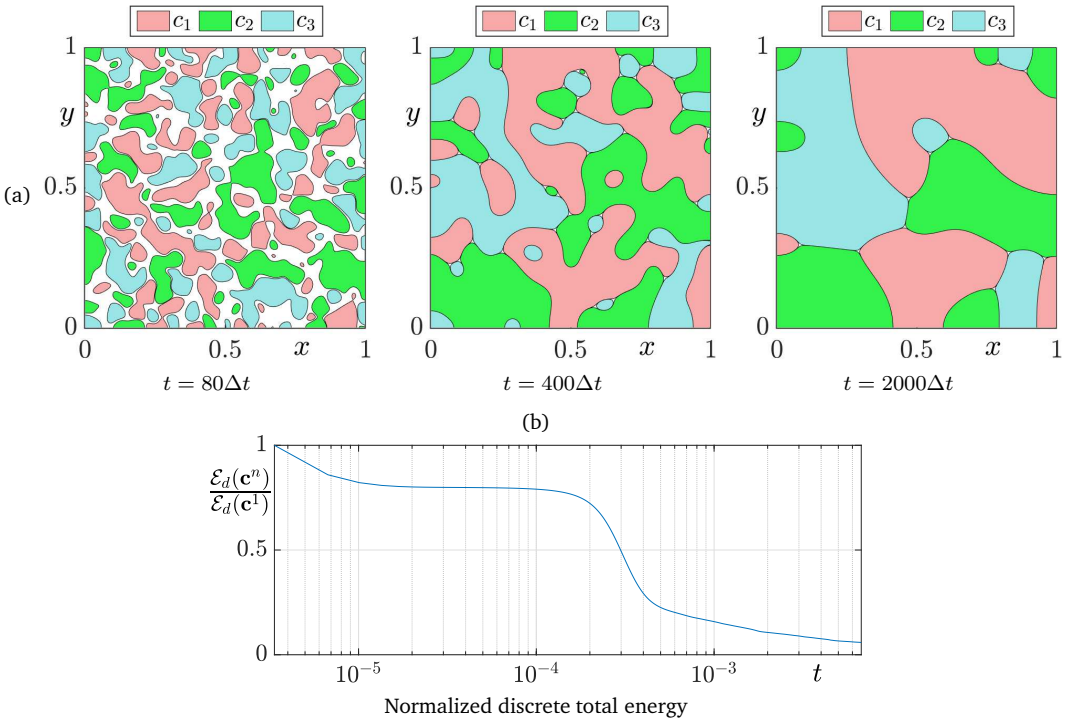

Figure 5: Snapshots of the computational solution at times $t = 80\Delta t$, $400\Delta t$, and $2000\Delta t$, and temporal evolution of the normalized discrete total energy.

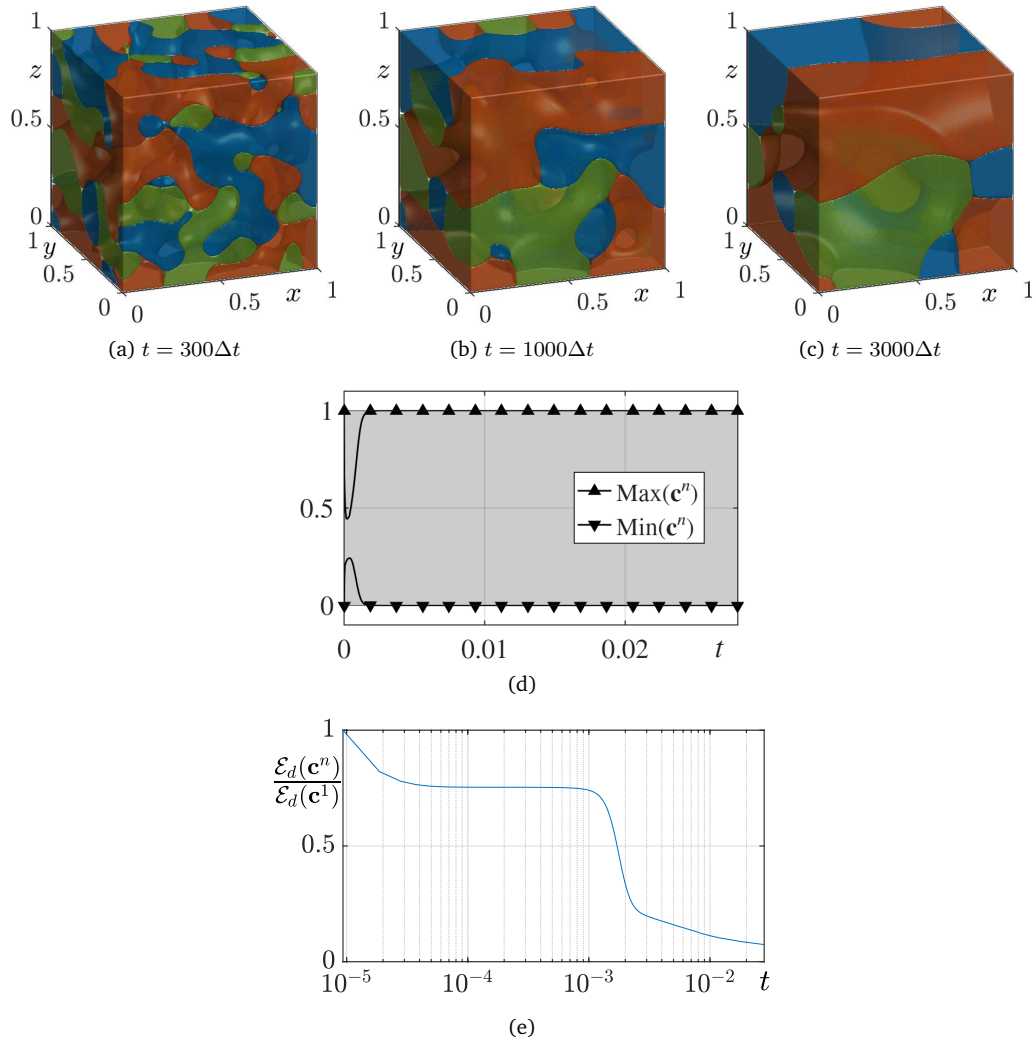

Figure 6: Snapshots of the numerical solutions at $t = 300\Delta t$, $1000\Delta t$, and $3000\Delta t$, and temporal evolutions of the maximum and minimum values of the solutions and the normalized discrete total energy.

computational solutions computed using the maximum time step for the fully explicit method are stable, which verifies that they satisfy the maximum principle. Fig. 6(e) presents the normalized discrete total energy, and we observe that the computational solutions satisfy the energy dissipation law.

5. Conclusions

In this study, we performed a stability analysis of the tAC equation when solved by the fully explicit Euler method. By directly analyzing the update formula and applying maximum principle arguments, we derived a sufficient condition on the time step size that guarantees the stability of the computational solution. This condition was proven

to be optimal in the sense that it provides the largest possible time step among all values that preserve the discrete maximum principle. To verify the sharpness of the derived condition, we constructed an initial condition under which the computational solution violates the maximum principle when the time step size exceeds the proposed bound. This result was rigorously proven through mathematical analysis, and it shows that instability indeed occurs beyond the threshold. In addition, numerical experiments were conducted to validate the theoretical findings. The results confirmed that the numerical solution remains stable and bounded within physically meaningful limits when the time step satisfies the derived condition. Furthermore, it was observed that, under this condition, the explicit Euler method preserves the energy dissipation law of the tAC equation. Overall, this study provides a theoretical analysis of the stability limit for applying the fully explicit Euler method to ternary phase-field models. While many previous studies have focused on implicit or energy-stable methods, we investigated the explicit Euler method, which is simple to implement and computationally inexpensive, and derived an explicit condition on the time step size. These results may contribute to the development of stable and efficient explicit numerical methods for multi-component phase-field models, where preserving physical constraints such as the maximum principle and energy dissipation plays an important role. In future work, we will focus on developing a maximum-principle-preserving and energy-stable high-order scheme for the tAC equation by referring to high-order methods such as the second-order leap-frog FDM [3] and the additive partitioned Runge-Kutta scheme [47]. In contrast to choosing an arbitrarily small time step by trial and error to maintain stability, or using a time step that initially appears stable but eventually causes the numerical solution to blow up, the proposed maximum time step guarantees that the numerical solution remains stable and can be computed with optimal efficiency. Moreover, in large-scale computations that require long simulation times, the proposed condition can play an essential role in ensuring the stability and accuracy of numerical solutions, which is especially important for parallel computations and other high-performance computing environments.

Acknowledgments

The authors would like to thank the reviewers for their constructive comments and valuable suggestions, which have greatly improved the quality of this paper.

Y.J. Hwang was supported by the National Research Foundation of Korea (NRF) grant funded by the Korea government (MSIT) (No. RS-2025-00562584). J.S. Kim was supported by the National Research Foundation of Korea (NRF) grant funded by the Korea government(MSIT) (No. 2022R1A2C1003844).

References

[1] S. M. Allen and J. W. Cahn, *A microscopic theory for antiphase boundary motion and its application to antiphase domain coarsening*, Acta Metall. 27 (1979), 1085–1095.

[2] Y. CHEN, X. LIU, Z. CHAI, AND B. SHI, *Regularized lattice Boltzmann method based maximum principle and energy stability preserving finite-difference scheme for the Allen-Cahn equation*, J. Comput. Phys. 528 (2025), 113831.
[3] Y. CHEN, F. QIN, Z. DU, AND T. HOU, *A maximum bound principle preserving and energy-stable second-order leap-frog finite difference scheme for the Allen-Cahn equation with a general mobility*, Int. J. Comput. Math. 102 (2025), 1318–1332.
[4] D. A. COGSWELL AND W. C. CARTER, *Thermodynamic phase-field model for microstructure with multiple components and phases: The possibility of metastable phases*, Phys. Rev. Ev 83 (2011), Paper No. 061602.
[5] C. K. DOAN, T. T. P. HOANG, AND L. JU, *Fully discrete error analysis of first-order low regularity integrators for the Allen-Cahn equation*, Numer. Methods Partial Differ. Equ. 39 (2023), 3594–3608.
[6] Z. DU AND T. HOU, *A linear second-order maximum bound principle preserving finite difference scheme for the generalized Allen-Cahn equation*, Appl. Math. Lett. 158 (2024), Paper No. 109250.
[7] H. GARCKE, B. NESTLER, AND B. STOTH, *On anisotropic order parameter models for multi-phase systems and their sharp interface limits*, Physica D 115 (1998), 87–108.
[8] Y. GENG, O. BURKOVSKA, L. JU, G. ZHANG, AND M. GUNZBURGER, *An end-to-end deep learning method for solving nonlocal Allen-Cahn and Cahn-Hilliard phase-field models*, Comput. Methods Appl. Mech. Eng. 436 (2025), Paper No. 117721.
[9] S. HAM, J. YANG, Y. HWANG, AND J. KIM, *A novel multi-component Allen-Cahn system for reducing the vacuum phenomenon at the triple junction*, AIP Adv. 15 (2025), Paper No. 035311.
[10] X. HU, Q. XIA, B. XIA, AND Y. LI, *A second-order accurate numerical method with unconditional energy stability for the Lifshitz-Petrich equation on curved surfaces*, Appl. Math. Lett. 163 (2025), Paper No. 109439.
[11] D. JEONG, J. YANG, AND J. KIM, *A practical and efficient numerical method for the Cahn-Hilliard equation in complex domains*, Commun. Nonlinear Sci. Numer. Simul. 73 (2019), 217–228.
[12] J. JI, C. ZHANG, S. LI, M. CHEN, AND Z. XIE, *Simulation of $M_{23}C_6$ precipitation mechanism during solidification of Ni40A coated on phosphorus removal roll by phase field method*, Appl. Phys. A 129 (2023), Paper No. 618.
[13] J. JIANG, K. GARIKIPATI, AND S. RUDRARAJU, *A diffuse interface framework for modeling the evolution of multi-cell aggregates as a soft packing problem driven by the growth and division of cells*, Bull. Math. Biol. 81 (2019), 3282–3300.
[14] J. KIM AND H. G. LEE, *A new conservative vector-valued Allen-Cahn equation and its fast numerical method*, Comput. Phys. Commun. 221 (2017), 102–108.
[15] S. KWAK, *Practical implementation of boundary conditions in the Thomas algorithm*, J. KSIAM, 29(2) (2025), 171–183.
[16] K. F. LAM AND R. WANG, *Stability and convergence of relaxed scalar auxiliary variable schemes for Cahn–Hilliard systems with bounded mass source*, J. Numer. Math. 32 (2024), 233–255.
[17] H. LI, J. YANG, AND W. ZHANG, *Analysis and numerical methods for nonlocal-in-time Allen-Cahn equation*, Numer. Methods Partial Differ. Equ. 40 (2024), Paper No. e23124.
[18] J. LI AND J. LI, *Unconditional MBP preservation and energy stability of the stabilized exponential time differencing schemes for the vector-valued Allen-Cahn equations*, Commun. Nonlinear Sci. Numer. Simul. 139 (2024), Paper No. 108271.
[19] Y. LI, R. LIU, Q. XIA, C. HE, AND Z. LI, *First- and second-order unconditionally stable direct*

discretization methods for multi-component Cahn-Hilliard system on surfaces, J. Comput. Appl. Math. 401 (2022), Paper No. 113778.

[20] Y. Li, K. Qin, Q. Xia, and J. Kim, *A second-order unconditionally stable method for the anisotropic dendritic crystal growth model with an orientation-field*, Appl. Numer. Math. 184 (2023), 512–526.

[21] H. Liang, H. Liu, Z. Chai, and B. Shi, *Lattice Boltzmann method for contact-line motion of binary fluids with high density ratio*, Phys. Rev. E 99 (2019), Paper No. 063306.

[22] L. Liu, X. Xiao, and X. Feng, *The stabilized finite element method for the Cahn-Hilliard phase-field model of diblock copolymers on evolving surfaces*, Numer. Math. Theory Methods Appl. 18 (2024), 103–126.

[23] X. Liu, Q. Hong, H. L. Liao, and Y. Gong, *A multi-physical structure-preserving method and its analysis for the conservative Allen-Cahn equation with nonlocal constraint*, Numer. Algorithms 97 (2024), 1431–1451.

[24] Y. Lu, C. Yuan, and H. Guo, *Convolution tensor decomposition for efficient high-resolution solutions to the Allen-Cahn equation*, Comput. Methods Appl. Mech. Eng. 433 (2025), Paper No. 117507.

[25] Z. Lv, X. Song, J. Feng, Q. Xia, B. Xia, and Y. Li, *Reduced-order prediction model for the Cahn-Hilliard equation based on deep learning*, Eng. Anal. Bound. Elem. 172 (2025), Paper No. 106118.

[26] B. Nestler, H. Garcke, and B. Stinner, *Multicomponent alloy solidification: Phase-field modeling and simulations*, Phys. Rev. E 71 (2005), Paper No. 041609.

[27] A. Novick-Cohen, *Triple-junction motion for an Allen-Cahn/Cahn-Hilliard system*, Physica D 137 (2000), 1–24.

[28] D. A. Porter and K. E. Easterling, *Phase Transformations in Metals and Alloys (revised reprint)*, CRC Press, (2009).

[29] M. A. Rasolofomanana, R. Le Tellier, and H. Henry, *Rise and fall of a multicomponent droplet in a surrounding fluid: Simulation study of a bumpy path*, Phys. Rev. Fluids 10 (2025), Paper No. 023601.

[30] D. A. Rueda-Gómez, E. E. Rueda-Fernández and É. J. Villamizar-Roa, *Numerical analysis for a non-isothermal incompressible Navier-Stokes-Allen-Cahn system*, J. Math. Fluid Mech. 26 (2024), Paper No. 63.

[31] X. Song, Q. Xia, J. Kim, and Y. Li, *An unconditional energy stable data assimilation scheme for Navier-Stokes-Cahn-Hilliard equations with local discretized observed data*, Comput. Math. Appl. 164 (2024), 21–33.

[32] X. Song, B. Xia and Y. Li, *An efficient data assimilation based unconditionally stable scheme for Cahn-Hilliard equation*, Comput. Appl. Math. 43 (2024), Paper No. 121.

[33] L. Wang, K. He, and H. Wang, *Phase-field-based lattice Boltzmann model for simulating thermocapillary flows*, Phys. Rev. E 108 (2023), Paper No. 055306.

[34] Z. Wang, J. Zhang, and X. Yang, *Fully discrete spectral-Galerkin scheme for a ternary Allen-Cahn type mass-conserved Nakazawa-Ohta phase-field model for triblock copolymers*, J. Comput. Appl. Math. 419 (2023), Paper No. 114699.

[35] J. Wu, J. Yang, and Z. Tan, *Unconditionally energy-stable time-marching methods for the multi-phase conservative Allen-Cahn fluid models based on a modified SAV approach*, Comput. Methods Appl. Mech. Eng. 398 (2022), Paper No. 115291.

[36] Q. Xia, S. Lai, J. Kim, and Y. Li, *Phase field modeling of melting and solidification dynamics in metallic powders during the bed fusion process*, Commun. Nonlinear Sci. Numer. Simul. 115 (2025), Paper No. 108762.

[37] Q. Xia, Y. Liu, J. Kim, and Y. Li, *Binary thermal fluids computation over arbitrary surfaces*

with second-order accuracy and unconditional energy stability based on phase-field model, J. Comput. Appl. Math. 433 (2023), Paper No. 115319.

[38] Q. XIA, J. YANG, AND Y. LI, *On the conservative phase-field method with the N-component incompressible flows*, Phys. Fluids 35 (2023), Paper No. 013102.

[39] W. XIE, Z. WANG, J. KIM, X. SUN, AND Y. LI, *A novel ensemble Kalman filter based data assimilation method with an adaptive strategy for dendritic crystal growth*, J. Comput. Phys. 524 (2025), Paper No. 113711.

[40] W. XIE, Q. XIA, Q. YU, AND Y. LI, *An effective phase field method for topology optimization without the curvature effects*, Comput. Math. Appl. 146 (2023), 200–212.

[41] X. YANG, *Efficient, second-order in time, and energy stable scheme for a new hydrodynamically coupled three components volume-conserved Allen-Cahn phase-field model*, Math. Models Methods Appl. Sci. 31 (2021), 753–787.

[42] X. YANG AND X. HE, *A fully-discrete decoupled finite element method for the conserved Allen-Cahn type phase-field model of three-phase fluid flow system*, Comput. Methods Appl. Mech. Eng. 389 (2022), Paper No. 114376.

[43] V. YUSHUTIN, A. QUAINI, S. MAJD, AND M. OLSHANSKII, *A computational study of lateral phase separation in biological membranes*, Int. J. Numer. Method Biomed. Eng. 35 (2019), Paper No. e3181.

[44] S. ZHAI, Z. WENG, Y. MO, AND X. FENG, *Energy dissipation and maximum bound principle preserving scheme for solving a nonlocal ternary Allen-Cahn model*, Comput. Math. Appl. 155 (2024), 150–164.

[45] H. ZHANG, X. QIAN, AND S. SONG, *Third-order accurate, large time-stepping and maximum-principle-preserving schemes for the Allen-Cahn equation*, Numer. Algorithms 95 (2024), 1213–1250.

[46] J. ZHANG AND X. YANG, *Unconditionally energy stable large time stepping method for the L2-gradient flow based ternary phase-field model with precise nonlocal volume conservation*, Comput. Methods Appl. Mech. Eng. 361 (2020), Paper No. 112743.

[47] W. ZHANG, X. GU, W. CAI, AND Y. WANG, *Maximum bound principle preserving additive partitioned Runge-Kutta schemes for the Allen-Cahn equation*, J. Comput. Phys. 516 (2024), Paper No. 113279.

[48] Y. ZHANG, B. DONG, X. AN, Y. WANG, X. ZHOU, AND W. LI, *Phase-field-based lattice Boltzmann model for ternary fluid flows considering the wettability effect*, Appl. Math. Model. 103 (2022), 195–220.